DOI: 10.53992/njns.v11i1.306 NUST Journal of Natural Sciences, Vol. 11, Issue 1, 2026

Research Article

Green synthesis of iron nanoparticles using Agaricus bisporus: Evaluation of antifungal and antidiabetic potential

Ammara Zaidi[1], Munaza Kiran[1], Aeysha Sultan[2*], Noreen Sajjad[3], Roberto Acevedo[4]

[1]Department of Botany, Division of Science & Technology, University of Education, Lahore, Pakistan.
[2*]Department of Chemistry, Division of Science & Technology, University of Education, Lahore, Pakistan.
[3]Department of Chemistry, the University of Lahore, 1-km, Defense Road, Lahore-Pakistan.
[4]Facultad de Ingeniería. Universidad San Sebastián. Bellavista 7. 8420524. Santiago. Chile (RA).

***Corresponding author's email:** ayesha.sultan@ue.edu.pk

Abstract

This study explores the green synthesis of iron nanoparticles (FeNPs) using aqueous extracts of *Agaricus bisporus* (stipe and pileus) and evaluates their antifungal and antidiabetic potential. FeNPs were synthesized at room temperature and under heating conditions, with characterization performed using UV-visible spectroscopy, FTIR, SEM-EDS, and DLS. The formation of FeNPs was confirmed by a color shift to amber and a characteristic absorption peak at 450 nm. FTIR analysis revealed functional groups such as O-H, C=O, and Fe-O, indicating the involvement of mushroom phytochemicals in nanoparticle stabilization. SEM confirmed uniform morphology, with smaller FeNPs (35 nm) achieved using pileus extract (PE) under heating. Antifungal activity against *Aspergillus terreus* and *Aspergillus niger* was demonstrated *via* agar well diffusion assays, with inhibition zones up to 34 mm. FeNPs also exhibited significant antidiabetic potential, with glucose adsorption capacities up to 69% and α-amylase inhibition up to 77%, particularly for smaller nanoparticles. The study highlights the dual functionality of *A. bisporus*-derived FeNPs, showcasing their promise as sustainable nanomaterials for biomedical applications.

Keywords: Green Synthesis, Mycosynthesis, *Agaricus Bisporus, Aspergillus Terreus*, Iron Nanoparticles, Antifungal, Antidiabetic, Alpha-Amylase Inhibitory Assays.

Article History: **Received:** 12 Jan 2026, **Revised:** 27 Mar 2026, **Accepted**: 28 Mar 2026, **Published:** 07 Apr 2026.

Introduction

Nanomaterials, due to their small size (within the nano-range, 1–100 nm), have gained tremendous importance in recent decades owing to their unique physical, chemical, and biological properties, which differ significantly from those of bulk materials [1 - 4]. Their high surface-area-to-volume ratio and quantum confinement effects contribute to enhanced reactivity, making them suitable for advanced

applications in catalysis, medicine, and environmental remediation [1, 5].

Among various metal nanoparticles (NPs), iron nanoparticles (FeNPs) are highly explored due to their exceptional magnetic properties, thermal and electrical conductivity, and dimensional stability [2, 5]. Conventionally, FeNPs are synthesized using chemical methods that involve energy-intensive processes and hazardous reducing agents such as sodium borohydride ($NaBH_4$) or hydrazine (N_2H_4) [6, 7]. However, growing environmental concerns have shifted research toward green synthesis approaches that utilize plant extracts, fungi, or bacteria as sustainable alternatives [3, 8 - 9].

Compared to bacteria and plants, fungi-derived metabolites are superior reducing and stabilizing agents due to their high metal-chelating capacity, low nutritional requirements, and adaptability to extreme conditions [3, 10]. Mushrooms, in particular, are rich in bioactive compounds such as polysaccharides, phenolics, and proteins, which facilitate the reduction and stabilization of metal ions into nanoparticles [11, 12].

The edible mushroom *Agaricus bisporus* (white button mushroom) is widely cultivated and contains essential nutrients, including dietary fiber, vitamins (thiamine, riboflavin, niacin, biotin, ascorbic acid, cobalamin), and minerals (potassium, phosphorus) [13, 14]. Its high reducing potential has been successfully employed in the synthesis of silver (AgNPs) and copper nanoparticles (CuNPs) [15]. However, its application in the green synthesis of FeNPs remains unexplored.

This study aims to optimize the reaction conditions for synthesizing FeNPs using *A. bisporus* extract and evaluate their antifungal and antidiabetic potential.

Experimental materials

A. bisporus (White button mushroom) was purchased from a local store "House of mushroom" (Johar town, Lahore). Ferric chloride ($FeCl_3$) used in the work was of analytical grade and obtained from Sigma Aldrich(USA) and distilled water was obtained from Research Lab, University of Lahore, Lahore, Pakistan.

Characterization

Fourier-Transform Infrared Spectroscopy (FTIR) was employed to study the various vibrational modes and analyze the metal-organic interlinkage. FTIR was used to determine the organic functional groups linked to the surface of FeNPs. The dried samples were analyzed by FTIR after mixing with a finely powdered KBr. The samples were scanned in the 4000-500 cm^{-1} spectral range with a resolution of 16 cm^{-1} (Fig**.** 3B).[16]. The NPs' morphology and size distribution was observed using SEM (H-7600, Hitachi Ltd. Tokyo, Japan). The sample's structure was inspected by applying Raman spectroscopy. The sample's absorption range and properties were assessed through ultraviolet-visible diffuse reflectance spectroscopy (UV-VIS DRS). Energy Dispersive X-Ray Analysis (EDX) is used for elemental analysis. EDX is coupled with electron microscopy instruments (Scanning electron microscopy (SEM)). Moreover, Dynamic Light Scattering (DLS) Analysis used for the Zeta sizer was used to determine the particle size and zeta potential of iron nanoparticles (FeNPs). Phosphate-buffered saline (0.15 M, pH 7.2) was used to dilute the lyophilized samples ten times. The aliquots were then sampled in DLS cuvettes, and the equivalent diameters, size distribution, and zeta potential of nanoparticles were determined. At room temperature (25 °C), particle sizes were measured at a scattering angle of 90°.[16].

Preparation of mushroom extract

A. bisporus was washed thoroughly with

distilled water to get rid of dirt and mud that had adhered to the mushroom's surface. The stipe and pileus were separately cut into tiny pieces. 5 grams each of stipe and pileus were separately boiled in 100 ml distilled water for 10 min and then filtered by using Whatmann No.1 filter paper to afford stipe extract (SE) and Pileus extract (PE). The extracts were preserved in airtight containers until further use.[17].

Synthesis of iron nanoparticles

Method 1: Mycosynthesis at room temperature

Different concentrations of $FeCl_3$ aqueous solutions (0.5, 1.0, 1.5, 2.0, and 2.5 mM) were prepared for nanoparticle synthesis. In each reaction, 5 mL of $FeCl_3$ solution was placed in a 150 mL Erlenmeyer flask under continuous stirring, followed by the addition of varying volumes (1-5 mL) of stipe extract (SE). The total reaction volume was brought to 50 mL by supplementing with distilled water. The mixtures were then incubated at 37°C for 48 hours under ambient conditions, during which the color transition from lemon yellow to black indicated successful formation of iron nanoparticles. The resulting FeNPs were isolated by centrifugation at 8000 rpm for 20 minutes at 4°C. After discarding the supernatant, the obtained pellet was washed with acetone to remove residual reactants and subsequently air-dried at room temperature for further characterization (Figure 1e).

Method 2: Mycosynthesis by heating the reaction mixture until dryness

For the heat-assisted synthesis method, varying volumes (1-5 mL) of pileus extract (PE) were introduced into 5 mL aliquots of $FeCl_3$ solutions (0.5-2.5 mM) in 150 mL Erlenmeyer flasks under constant stirring. The reaction mixtures were subsequently diluted to a final volume of 50 mL using distilled water. These solutions were then subjected to controlled heating at 80°C using a hot plate with magnetic stirring until complete solvent evaporation was achieved, yielding FeNPs as dark brown to black powders (Fig. 1f) [18].

Evaluation of antifungal activity

Agar plate's preparation

4 grams of Commercial potato dextrose agar (PDA) was added in 100 ml of distilled water in an Erlenmayer's flask. The agar was dissolved by stirring the mixture on a hotplate with a magnetic bar. The petri plates were cleaned and stacked in a plastic bag. The agar solution, petri plates and microtips were autoclaved at 121℃ to sterilize all the ingredients prior to preparing culture media. After sterilization, the agar solution was poured into the petri plates (approx. 20 ml) in a laminar air hood. The lid of the plates was slightly opened to solidify the agar. In 20-25 minutes, the plates were completely solidified. The Petri plates were sealed with scotch tape and stored upside down for 24 hours at 28-35℃.[19].

Determination of morphological characters of pure cultures

The inoculums of the pathogenic fungi (*Aspergillus terreus* and *Aspergillus niger)* were taken from the laboratory of Department of Botany University of Education, Lahore. The pathogen was placed on PDA media with a sterilized inoculating loop. The petri plates were incubated at 37℃ for 7 days. The morphological characteristics, i.e., diameter, surface color, margins, reverse side and elevations, were determined.[20].

Microscopic analysis of the pathogens

A drop of glycerine was poured in the middle of the glass slide. A small amount of the pathogen was placed on the liquid using a sterile tweezer. One side of the coverslip

was placed at an angle against the slide, contacting the outside edge of the liquid drop. The cover slip was slowly lowered to avoid air bubbles. By using tissue paper, any extra water was removed. The specimens were observed microscopically at 10×, 40×, and 100×, and photographs were taken.[20].

Evaluation of antifungal activity

The agar well diffusion technique was used to check the antifungal activity of the microbiologically synthesized FeNPs against *A. niger* and *A. terreus*. These organisms were cultured in PDA medium in an incubator at 37°C and using a sterile inoculating loop, the test organisms were swabbed on the agar plates. Sterile microtips were used to create wells in petri plates. Different concentration of synthesized FeNPs solution (20μl, 40μl, 60μl and 100μl) was placed in each well. Following inoculation, the plates were incubated at room temperature for 7 days. Dermosporin (broad spectrum antimycotic drug) was used as a control. The zone of inhibition was measured in mm. The creation of a clear zone surrounding the well was considered an antifungal action by the FeNPs.[16].

Results and discussion

Biosynthesis of iron nanoparticles

Mushrooms represent a valuable natural source of bioactive compounds, exhibiting well-documented pharmacological properties including anti-inflammatory, antibacterial, antioxidant, antifungal, antiviral, anticancer, cardiovascular, hypotensive, and hepatoprotective activities [21]. This rich phytochemical profile makes mushroom extracts ideal for the green synthesis of iron nanoparticles (FeNPs), offering a cost-effective, biocompatible, and environmentally benign approach to nanomaterial production. The biosynthesis process was visually monitored through distinct colorimetric changes, where the characteristic amber coloration specifically developed in reaction flasks containing both mushroom extract and $FeCl_3$ solution. This selective color transformation, emerging within 48 hours of incubation, serves as a reliable indicator of FeNP formation, attributable to the reduction potential of mushroom phytochemicals and the subsequent excitation of surface plasmon resonance in the synthesized nanoparticles [22]. The absence of such color changes in control solutions confirms the essential role of mushroom-derived reducing agents in the nanoparticle formation process. (Fig 1).

Figure. 1: A) *A. bisporus*; B). SE; C). PE; D) Different concentrations of $FeCl_3$ solution; E) Synthesized Iron nanoparticle solutions under room temperature conditions; F) Air dried iron nanoparticles prepared by heating to complete dryness.

Upon reaction of A. bisporus stipe (SE) and pileus (PE) extracts (1-5 mL) with $FeCl_3$ solutions (0.5-2.5 mM), a progressive color transition was observed, evolving from initial pale yellow to a distinct amber hue. This chromatic transformation, visible within 48 hours of incubation and reaching maximum intensity by 72 hours (Fig. 2), serves as a visual indicator of iron nanoparticle formation. The time-dependent development of coloration corresponds to the gradual reduction of Fe^{3+} ions and subsequent nanoparticle nucleation and growth processes. Figure 2 clearly demonstrates this progression, showing (a) the original pale yellow reaction mixture and (b) the characteristic

amber coloration after 48 hours, providing visual confirmation of successful nanoparticle synthesis.

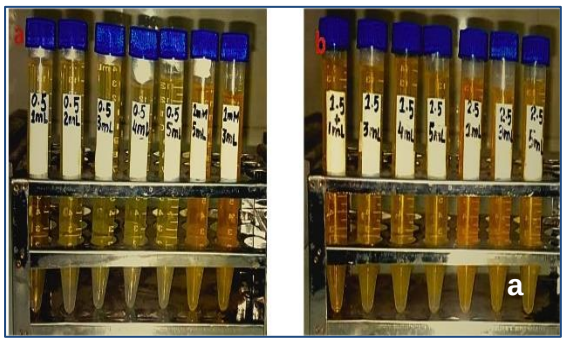

Figure. 2: Color of reaction mixture: a) before reaction; b) after 48 hours.

The UV-Visible absorbance spectra (Fig. 3) demonstrate the successful formation of FeNPs through bioreduction using *Agaricus bisporus* extracts. The spectra show characteristic absorption peaks near 450 nm for all samples, corresponding to the typical surface plasmon resonance (SPR) of FeNPs [23 - 27]. Distinct variations in absorbance intensity are evident among the different samples: PE155 and SE051 exhibit stronger absorption, indicating the presence of smaller nanoparticles with higher surface area, while SE255 shows relatively lower absorption, suggesting larger particle sizes or aggregates. The pileus extract-derived samples (PE155, PE154) display comparable absorption profiles to those synthesized using stipe extract (SE051, SE101, SE251, SE255), confirming consistent reduction capabilities of both mushroom parts. The absence of multiple peaks or significant peak broadening suggests uniform nanoparticle formation without substantial oxidation or aggregation. These spectral features collectively verify the effective biosynthesis of FeNPs with size-dependent optical properties that correlate with the synthetic conditions employed for each sample. The reproducibility of the SPR band position across all samples further confirms the stability of the green synthesis approach.

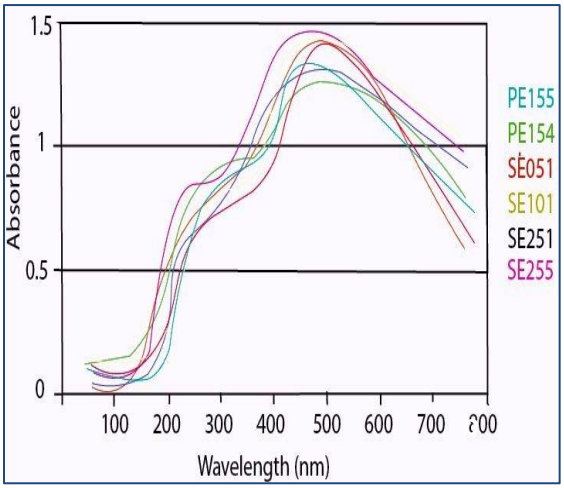

Figure. 3: UV-Visible spectra of some selective FeNPs.

FTIR studies

The FTIR spectrum of FeNPs synthesized using A. bisporus extract (Fig. 4) reveals characteristic vibrational modes of both organic capping agents and the iron oxide core. A broad absorption band in the 3200-3350 cm^{-1} region corresponds to O-H stretching vibrations from polyphenols and polysaccharides present in the mushroom extract. The spectrum shows prominent peaks at 1620-1600 cm^{-1} (carbonyl C=O stretching) and 1390-1450 cm^{-1} (C=C aromatic stretching), confirming the presence of bioactive mushroom compounds coating the nanoparticles. A distinct signal at 1030-1150 cm^{-1} arises from C-O stretching vibrations of alcoholic or ether groups. Most significantly, the appearance of a strong Fe-O stretching vibration at 570 cm^{-1} provides direct evidence of iron oxide nanoparticle formation [28, 29]. The transmittance spectrum (Fig. 4) clearly displays these characteristic bands, with the Fe-O vibration showing particularly strong absorption, indicating successful nanoparticle synthesis. The spectral features between 4000-500 cm^{-1} collectively demonstrate the dual nature of the biosynthesized nanoparticles, featuring both organic phytochemical coatings from the mushroom extract and an inorganic iron oxide core.

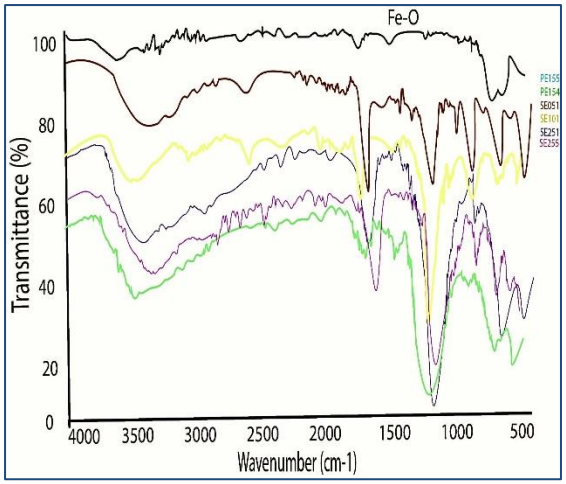

Figure 4: FTIR spectrum of synthesized Fe-NP.

The FTIR spectra of FeNPs synthesized under different conditions reveal distinct surface chemistries influenced by both biomolecular capping and thermal effects. For nanoparticles prepared at room temperature, the broad O–H stretching band (3200–3350 cm^{-1}) arises from hydroxyl groups in mushroom-derived polyphenols (e.g., flavonoids) and polysaccharides (e.g., β-glucans), which act as both reducing and stabilizing agents [28, 30]. The carbonyl stretch (1620–1600 cm^{-1}) likely originates from amide I bands of proteins and phenolic acids, while the C–O vibration (1030–1150 cm^{-1}) suggests glycosidic linkages in polysaccharides [31]. Notably, the Fe–O vibration at 570 cm^{-1} confirms the formation of magnetite (Fe_3O_4) or maghemite (γ-Fe_2O_3) phases, consistent with biosynthetic routes [32]. In heat-assisted synthesis, the spectral shifts (O–H attenuation, C=C intensification at 1450 cm^{-1}) align with pyrolytic decomposition of organics, potentially forming graphitic shells that enhance nanoparticle stability, as reported in thermal green synthesis methods [33]. The preserved Fe–O peak indicates thermal stability of the iron oxide core up to the applied temperatures.

Particle size control is governed by competing kinetic and thermodynamic factors. Higher $FeCl_3$ concentrations (0.5–2.5 mM) accelerate nucleation rates (LaMer mechanism), but excess Fe^{3+} ions promote aggregation through reduced steric stabilization by mushroom phytochemicals [34]. This is evidenced by DLS data showing a 40-60 nm size increase at 2.5 mM versus 0.5 mM $FeCl_3$ (Fig. 7). The temperature dependence follows Arrhenius principles – room-temperature synthesis allows gradual Oswald ripening (favoring monodispersity), while rapid solvent evaporation during heating kinetically traps smaller nuclei (20-30 nm) before aggregation occurs [35]. Comparative studies suggest stipe extracts (SE) yield smaller particles than pileus (PE), possibly due to higher protein content (e.g., lectins) providing stronger electrostatic stabilization [36]. These findings align with recent work on fungal-mediated synthesis, where extract composition and processing parameters jointly determine nanoparticle properties [37, 38].

Size determination of FeNPs

The particle sizes of Fe nanoparticles were evaluated using DLS. The size of Fe nanoparticles is typically influenced by the concentration of the precursor Fe (III) ions, the concentration of extract used, and the reaction conditions used.[39, 40] The nanoparticles were prepared by using different volumes (1-5mL) of SE and PE with different concentrations (0.5, 1.0, 1.5, 2.0 and 2.5 mM) of $FeCl_3$. The solutions after mixing the $FeCl_3$ solution with mushroom extracts were either stirred at room temperature or stirred under heating conditions till complete evaporation of solvent and conversion of the reaction mixture into fine powder. The nanoparticles thus prepared were analyzed by means of DLS to compare their sizes/hydrodynamic diameter using de-ionized H_2O as solvent. It was observed that when higher concentrations of $FeCl_3$ were used in the Synthesis of Fe nanoparticles, the size of the resulting nanoparticles were higher than the nanoparticles obtained with lower concentration of $FeCl_3$ (Fig. 5).

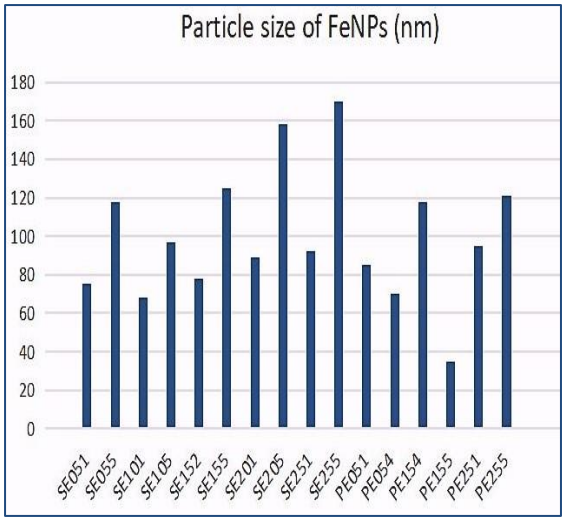

Figure5: Particle size analysis of FeNPs by DLS.

The expected size range of FeNPs prepared by using *A. bisporous* extract and $FeCl_3$ solution under stirring and subsequent centrifugation were smaller than the nanoparticles prepared by heating the solution to complete dryness. When *A. bisporous* extract and $FeCl_3$ solution were stirred together, the reduction of Fe (III) ions and the formation of Fe nanoparticles occur simultaneously. The nanoparticles form and grow in the solution, and as the reaction proceeds, they tend to aggregate and form larger clusters. During the centrifugation process, smaller nanoparticles that are well-dispersed in the solution are more likely to be recovered in the centrifuged sample, resulting in a smaller average particle size range. On the other hand, when the solution of $FeCl_3$ and *A. bisporous* extract is heated to complete dryness, the Fe nanoparticles tend to aggregate and form larger clusters due to the lack of dispersing forces. The studies at room temperature involved use of SE while in case of heating method PE were utilized. The findings of these studies are summarized in Table 1.

Table 1: FTIR and DLS results of synthesized Fe-NPs by SE & PE.

Entry	Conc of $FeCl_3$	Extract	Vol. of extract	Reaction conditions	Particle size	FTIR stretching frequency (cm^{-1})				
						O-H	C=O	C=C	C-O	Fe-O
SE051	0.5mM	SE	1ml	Centrifugation/RT	75	3340	1634	1448	1035	557
SE052			2ml		80	3280	1630	1437	1043	561
SE053			3ml		94	3242	1632	1428	1080	565
SE054			4ml		110	3258	1641	1434	1054	576
SE055			5ml		118	3294	1626	1450	1028	558
SE101	1.0mM	SE	1ml	Centrifugation/RT	68	3158	1627	1437	1035	569
SE102			2ml		75	3109	1630	1429	1041	558
SE103			3ml		80	3071	1625	1416	1021	567
SE104			4ml		88	3188	1629	1408	1036	564
SE105			5ml		97	3145	1638	1423	1028	586
SE151	1.5mM	SE	1ml	Centrifugation/RT	87	3235	1640	1468	1054	584
SE152			2ml		78	3250	1643	1439	1038	574
SE153			3ml		90	3227	1632	1476	1041	568
SE154			4ml		115	3235	1629	1468	1025	594
SE155			5ml		125	3235	1627	1457	1033	563
SE201	2.0mM	SE	1ml	Centrifugation/RT	89	3257	1640	1401	1032	572
SE202			2ml		91	3257	1640	1401	1029	577
SE203			3ml		94	3257	1640	1408	1033	564
SE204			4ml		120	3242	1640	1394	1028	569
SE205			5ml		158	3265	1640	1394	1025	573

Entry	Conc of $FeCl_3$	Extract	Vol. of extract	Reaction conditions	Particle size	FTIR stretching frequency (cm^{-1})				
						O-H	O-H	O-H	O-H	O-H
SE251	2.5mM	SE	1ml	Centrifugation/RT	92	3235	1632	1416	1039	558
SE252			2ml		97	3145	1625	1429	1028	567
SE253			3ml		106	3265	1640	1435	1025	583
SE254			4ml		135	3242	1640	1442	1023	577
SE255			5ml		170	3235	1640	1456	1068	569
PE051	0.5mM	PE	1ml	Heating till complete dryness	85	3341	1647	1449	1108	584
PE052			2ml		76	3338	1651	1453	1098	575
PE053			3ml		73	3344	1648	1449	1079	572
PE054			4ml		70	3308	1656	1440	1112	559
PE055			5ml		84	3328	1653	1444	1118	568
PE151	1.5mM	PE	1ml	Heating till complete dryness	90	3330	1658	1445	1121	553
PE152			2ml		96	3324	1648	1430	1126	564
PE153			3ml		110	3346	1652	1456	1118	574
PE154			4ml		118	3338	1650	1446	1124	581
PE155			5ml		35	3330	1644	1439	1119	587
PE251	2.5mM	PE	1ml	Heating till complete dryness	95	3347	1660	1446	1125	588
PE252			2ml		120	3365	1664	1455	1127	576
PE253			3ml		138	3394	1668	1441	1134	561
PE254			4ml		160	3397	1658	1444	1129	579
PE255			5ml		210	3405	1652	1456	1117	566

SEM studies

The surface morphology of FeNP with minimum particle size of 35 nm (PE155) as depicted by DLS was analyzed by SEM which indicated the particles to be uniform and granular. The Energy dispersive Xray analysis indicated the synthesized NPs to be primarily composed of Fe and O (Fig. 6A & 6B).

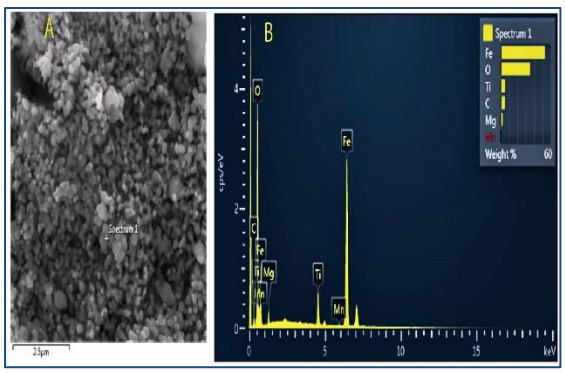

Figure. 6: A) SEM of PE155 ; B) EDX of PE155.

Determination of morphological characters of pure cultures

The surface color of *A. terreus* colonies was initially white. The colony appearance of *A. terreus* became golden yellow after 7 days of incubation. The reverse side is reddish/deep brown in color. The diameter of the colonies is in the range of 0.1-0.5 cm. The surface color of *A. niger* on PDA media appeared dark brown to black in color. The reverse side was creamy white. The elevations were umbonate and the diameter of the colonies are in the range of 0.5-2 cm (Table 2).

Antibacterial activity

Microscopic analysis of the pathogens

The conidia of *A. terreus* are small, globose-shaped, smooth-walled and yellowish in color.

Table 2: Colony morphology of *A. terreus* and *A. niger*.

Colony morphology							
Fungi	**Diameter of colony**	**Shape**	**Texture**	**Elevation**	**Surface color**	**Reverse color**	**Margins**
A. terreus	0.1-0.5cm	Punctiform	Rough	Umbonate	Initially white to pale yellow	Reddish brown	Entire
A. niger	0.5-2cm	Circular	Smooth	Umbonate	Dark brown to black	Creamy white	Entire

The conidiophores (spore-bearing structures) of *A. terreus* and *A. niger* are long and smooth, dark at the apex, and terminate in globose vesicles (Table 2 above; Fig. 7 below). In these species, the hyphae are septate, though *A. niger* specifically exhibits exine spiny ornamentation."

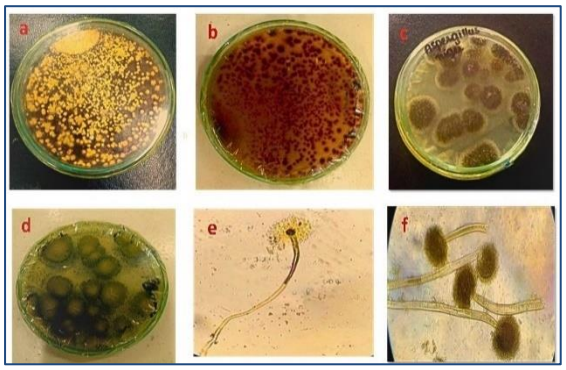

Figure. 7: a, b, c, & d: Obverse and reverse colony morphology of *A. terreus* and *A. niger*; e & f. microscopic view of *A. terreus* and *Aspergillus niger*.

Evaluation of antifungal activity

The iron nanoparticles synthesized from mushroom extracts were evaluated for antifungal efficacy against pathogenic fungus *A. terreus* and *A. niger* using the agar well-diffusion method and the zone of inhibition was calculated in millimetres (mm). In addition, the zone of inhibition of an antibiotic (Dermosporin) was measured. *A. bisporus* iron nanoparticles showed reduced antifungal efficacy against the selected pathogens. After 7 days incubation at 37°, inhibitory zones were discovered. Different concentration of the iron nanoparticle (0, 20, 40, 60, 80 and 100 μl) solutions were poured into the agar wells with the help of a micropipette. The plates were incubated for 7 days at 37°C and zone of inhibition was measured (Fig. 8). Table 3 indicates maximum zone of inhibition obtained by using these concentrations of FeNPs.

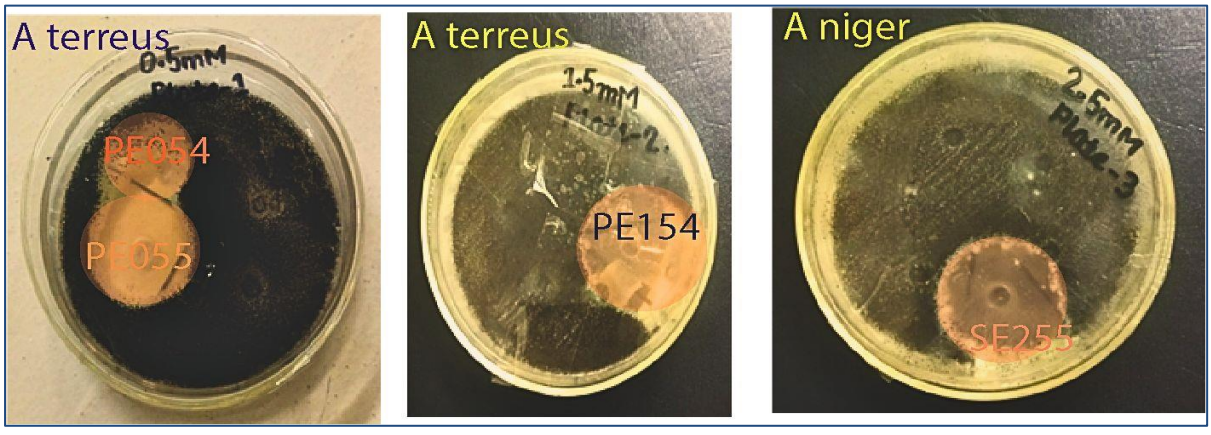

Figure. 8: Best fungicidal activity of synthesized iron nanoparticles observed against *A.terreus* and *A. niger*.

Table 3: Effect of different concentrations (20, 40, 60, 80 & 100$\boldsymbol{\mu l}$) of iron nanoparticles against A. terreus and A. niger.

Standard Drug/Sample	**Zone of inhibition (mm)**	
	Fungal strains	
	A. terreus	***A. niger***
Dermosporin	30.8± 0.50	46.4± 0.30
SE051	8.0 (100 µl)	10.0 (60 µl)
SE052	10 (100 µl)	12 (60 µl)
SE053	13 (100 µl)	18 (60 µl)
SE054	5 (100 µl)	25 (60 µl)
SE055	16 (60 µl)	23 (100 µl)
SE101	3.0 (100 µl)	8.0 (100 µl)
SE102	15 (80 µl)	15 (100 µl)
SE103	24 (60 µl)	11 (80 µl)
SE104	15 (100 µl)	5 (60 µl)
SE105	11 (60 µl)	0.0 (100 µl)
SE151	0 (100 µl)	5 (100 µl)
SE152	0 (100 µl)	8 (100 µl)
SE153	0 (100 µl)	9 (100 µl)
SE154	4 (100 µl)	13 (100 µl)
SE155	9 (100 µl)	16 (100 µl)
SE201	0 (100 µl)	13 (100 µl)
SE202	0 (100 µl)	15 (100 µl)
SE203	0 (100 µl)	11 (100 µl)
SE204	0 (100 µl)	17 (100 µl)
SE205	0 (100 µl)	20 (100 µl)
SE251	15 (100 µl)	19 (100 µl)
SE252	18 (100 µl)	21 (100 µl)
SE253	18 (100 µl)	24 (100 µl)
SE254	18 (100 µl)	29 (100 µl)
SE255	18 (100 µl)	32 (100 µl)
PE051	19 (100 µl)	21 (100 µl)

PE052	23 (100 µl)	26 (100 µl)
PE053	28 (100 µl)	27 (100 µl)
PE054	25 (100 µl)	31 (100 µl)
PE055	20 (100 µl)	34 (100 µl)
PE151	21 (100 µl)	23 (100 µl)
PE152	23 (100 µl)	25 (100 µl)
PE153	27 (100 µl)	28 (100 µl)
PE154	33 (100 µl)	30 (100 µl)
PE155	23 (100 µl)	29 (100 µl)
PE251	14 (100 µl)	19 (100 µl)
PE252	17 (100 µl)	16 (100 µl)
PE253	11 (100 µl)	13 (100 µl)
PE254	19 (100 µl)	9 (100 µl)
PE255	21 (100 µl)	7 (100 µl)

Evaluation of in vitro antidiabetic potential

Glucose adsorption assay

The ability of FENPs to adsorb glucose was evaluated by means of glucose adsorption following the method of Kaur etal.[30] Briefly, 0.1 g of the FeNPs was combined with a 10 mL of glucose (5–30 mM) solution. The resulting mixture was incubated at room temperature for 6 h followed by centrifugation at 8000 rpm at 4°C for 20 min (Table 4). The absorbance of glucose was determined at 520 nm before reaction and after 6 hours in order to determine the value of bound glucose by using the following formula:

$$Bound\ glucose = \frac{Glucose\ Conc\ before\ reaction - glucose\ conc\ after\ 6\ h}{sample\ weight} \times vol\ of\ sample$$

Alpha (α) amylase inhibition assay

Alpha-amylase is an enzyme which is responsible for hydrolyzing alpha bonds of polysaccharides to yield glucose and maltose. The action of this enzyme leads to elevation of blood glucose levels and its inhibition will lead to decrease in sugar level. The α-amylase inhibition assay was followed according to the procedure described briefly [28], a reaction mixture containing porcine pancreatic amylase (500 L) in phosphate-buffered saline (PBS), and FeNPs was prepared and kept at 37 C for 10 min. the reaction was initiated by adding 20 µl starch solution (1.0 mg/mL) and kept at ambient temperature for 0.5 hours (Table 4). The enzymatic reaction was quenched by adding HCL (20 µl, 1 M) and 100 µl iodine reagent was added and absorbance was recorded at 580 nm. The % of enzyme inhibition was calculated by following formula:

$$\%\ inhibition = \frac{Absorbance\ of\ Control - Absorbance\ of\ Sample}{Absorbance\ of\ Control} \times 100$$

Table 4: Antidiabetic activity of FeNPs.

Entry	Particle size of FeNPs (nm)	Glucose Adsorption			% Inhibition of α-amylase			
		5 mM glucose	15 mM glucose	30 mM glucose	20 µl/mL	40 µl/mL	60 µl/mL	100 µl/mL
PE	-	2%	4%	8%	14%	33%	42%	61%
SE	-	4%	5%	9%	16%	35%	44%	64%
Acorbose	-	40%	63%	87%	38%	46%	72%	83%
SE051	75	8%	13%	19%	20%	24%	28%	35%
SE055	118	6%	9%	13%	11%	15%	19%	24%
SE101	68	15%	19%	25%	24%	29%	30%	34%
SE105	97	9%	15%	28%	16%	22%	26%	29%
SE152	78	9%	14%	18%	19%	25%	29%	31%
SE155	125	5%	9%	11%	9%	16%	21%	15%
SE201	89	8%	13%	18%	14%	28%	33%	27%
SE205	158	4%	7%	10%	5%	10%	13%	20%
SE251	92	7%	11%	15%	13%	16%	19%	24%
SE255	170	2%	4%	7%	3%	8%	11%	17%
PE051	85	10%	16%	22%	16%	26%	34%	44%
PE054	70	13%	23%	34%	20%	29%	38%	52%
PE154	118	8%	15%	20%	12%	17%	23%	28%
PE155	35	23%	39%	69%	38%	49%	57%	77%
PE251	95	10%	14%	24%	17%	25%	33%	39%
PE255	121	7%	18%	30%	13%	18%	25%	31%

Antifungal potential

Fe-NPs interact with the fungal cell surfaces, affect their permeability and produce oxidative stress resulting in the inhibition of fungal growth.[41] This represents when the concentration of the nanoparticle solution is increased there may be a high oxidative stress which results in a large inhibition zone. *A. terreus* (34mm) showed a higher inhibition zone against 100μl standard antibiotic Dermosporin as compared to the *A. niger* (30mm). *Aspergillus niger* has high antifungal potential.

Antidiabetic potential

Analysis of glucose adsorption

Analysis of Glucose Adsorption by FeNPs and SE and PE extracts indicate that FeNPs have superior absorption potential as compared to extracts and interestingly, SE has higher adsorption potential as compared to PE. Also, table 4 indicated that glucose adsorption potential is closely related to particle size of the FeNPs; smaller the size higher the adsorption potential with best adsorption observed for PE155. It was also observed with glucose adsorption increased with increased molarity of glucose (Fig. 9) [30, 42 - 44].

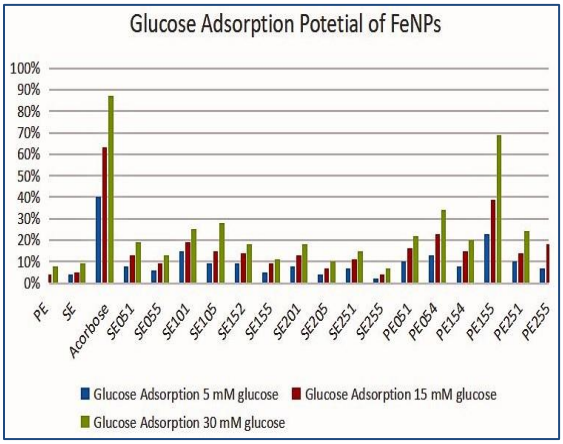

Figure 9: Glucose adsorption potential of FeNPs.

Inhibition of α-amylase

Amylases facilitate the breakdown of alpha-glycosidic bonds in starch and glycogen. The inhibition of amylase is recognized as a valuable tactic in managing carbohydrate metabolism disorders and associated conditions such as diabetes, obesity, and tooth decay.[30, 41] The alpha-amylase inhibitory effect was determined for FeNPs as well as Crude Extract (SE & PE). The percent inhibitory values of FeNPs at 20, 40, 60, 100 g/mL were noted (Fig.10). The results indicate the [45], SE has superior activity of PE. Furthermore, the inhibitory potential is dependent on size of NPs, smaller the size, higher the inhibitory potential of the FeNPs [46].

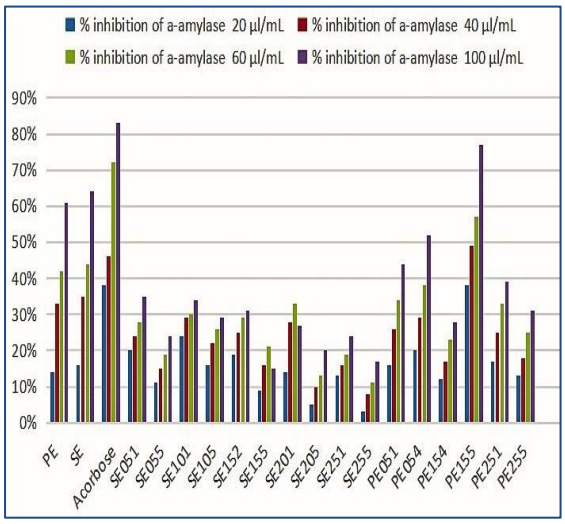

Figure 10: Amylase inhibitory potential of FeNPs.

Conclusions

This study successfully demonstrates facile *Agaricus bisporus* mediated mycosynthesis of FeNPs at room temperature and by heating until dryness. The FeNPs synthesized under different temperature conditions were characterized using UV-visible spectrophotometry, FTIR, SEM-EDS, and DLS, confirming their structural and compositional properties, including smaller size and uniform morphology, particularly under optimized conditions. The formation of FeNPs was indicated by an amber color and confirmed by UV-visible spectroscopy, with peak absorbance around 450 nm, and FTIR spectroscopy, revealing key functional groups like O-H, C=O, C=C, and Fe-O.

The synthesized FeNPs exhibited significant antifungal activity against *Aspergillus terreus* and *Aspergillus niger*, as demonstrated by clear inhibition zones in agar well diffusion assays. Additionally, the FeNPs showed promising antidiabetic potential through glucose adsorption and α-amylase inhibition, suggesting their multifunctional properties. Smaller-sized FeNPs displayed enhanced antifungal and antidiabetic activities, indicating the importance of optimizing synthesis parameters to tailor nanoparticle characteristics.

These findings support the potential of mushroom-derived FeNPs as multifunctional nanomaterials with diverse biomedical and environmental applications, including as antimicrobial agents and in diabetes management. Future research should focus on scaling up this green synthesis approach and exploring the full spectrum of their biomedical and environmental uses.

Declarations

Conflict of Interest

The authors declare that they have no conflict of interest.

Funding

This research did not receive any specific grant from funding agencies in the public, commercial, or not-for-profit sectors.

Availability of data and materials

The data that support the findings of this study are available from the corresponding author upon reasonable request.

References

1. Zhang XF, Liu ZG, Shen W, Gurunathan S. Nanoparticles in medicine: Therapeutic applications and developments. Clin Pharmacol Ther. 2016;99(3):252-265.
2. Wu W, He Q, Jiang C. Magnetic iron oxide nanoparticles: Synthesis and surface functionalization strategies. Nanoscale Res Lett. 2008;3(11):397-415.
3. Mohanpuria P, Rana NK, Yadav SK. Biosynthesis of nanoparticles: Technological concepts and future applications. J Nanopart Res. 2008;10(3):507-517.
4. Sharma VK, Sayes CM, Guo B, Pillai SD, Parsons JG, Hwang HM, Kuo GD. Nanomaterials in the environment: Behavior, fate, and remediation. Environ Sci Technol. 2019;53(10): 5583-5594.
5. Lu AH, Salabas EL, Schüth F. Magnetic nanoparticles: Synthesis, protection, functionalization, and application. Angew Chem Int Ed Engl. 2007;46(8):1222-1244.
6. Tartaj P, Morales MP, Veintemillas-Verdaguer S, Gonzalez-Carreño T, Serna CJ. The preparation of magnetic nanoparticles for applications in biomedicine. J Phys D Appl Phys. 2003;36(13):R182-R197.
7. Kumar B, Smita K, Cumbal L, Debut A. Green synthesis of iron nanoparticles using plant extracts: A review. Environ Chem Lett. 2020;18(5):1529-1548.
8. Iravani S. Green synthesis of metal nanoparticles using plants. Green Chem. 2011;13(10):2638-2650.
9. Mittal AK, Chisti Y, Banerjee UC. Biosynthesis of silver nanoparticles: Synthesis, mechanism, and medical applications. Adv Colloid Interface Sci. 2013;197-198:1-17.
10. Rai M, Yadav A, Gade A. Fusarium oxysporum-mediated biosynthesis of silver nanoparticles and their antibacterial activity. Nanomedicine (Lond). 2009;4(4):399-408.
11. Vigneshwaran N, Kathe AA, Varadarajan PV, Nachane RP, Balasubramanya RH. Biological synthesis of silver nanoparticles using the fungus Aspergillus flavus. Mater Lett. 2007;61(6):1413-1418.
12. Philip D. Biosynthesis of Au, Ag and Au–Ag nanoparticles using edible mushroom extract. Spectrochim Acta A Mol Biomol Spectrosc. 2009;73(2): 374-381.
13. Cheung PCK. Mini-review on edible mushrooms as source of dietary fiber: Preparation and health benefits. Food Chem. 2014;148:1-6.
14. Valverde ME, Hernández-Pérez T, Paredes-López O. Edible mushrooms: Improving human health and promoting quality life. Int J Microbiol. 2015; 2015:376387.
15. Sen IK, Maity K, Islam SS. Green synthesis of silver nanoparticles using Agaricus bisporus extract and their antibacterial activity. Int J Biol Macromol. 2013;62:439-445.
16. Mulvaney P. Surface plasmon spectroscopy of nanosized metal particles. Langmuir. 1996;12(3):788-800.
17. Manikandan G, Ramasubbu R. Biosynthesis of iron nanoparticles from Pleurotus florida and its antimicrobial activity against selected human pathogens. Int J Pharm Sci Res. 2021;12(1):475-481.
18. Batool F, Khurshid M, Kanwal Q, Shahzad K, Maqbool S, Shahid M, Akram W, Fatima N, Al-Qahtani WH, Al-Mutairi K. Biologically synthesized iron nanoparticles (FeNPs) from Phoenix dactylifera have anti-bacterial activities. Sci Rep. 2021;11(1):22132.
19. Salah Ud Din SHK, Haq S, Ahmad P, Khandaker MU, Faruque MRI, Idris AM, Sayyed MI. Bio-synthesized tin oxide nanoparticles: Structural, optical, and biological studies. Crystals. 2022;12(5):614.
20. Senanayake IC, Rathnayake AR,

Sandamali D, Calabon M, Gentekaki E, Lee HB, Pem D, Dissanayake L, Wijesinghe SN, Bundhun D, Nguyen TTT, Goonasekara ID, Abeywickrama PD, Jayawardena RS, Wanasinghe DN, Jeewon R, Bhat DJ, Xiang MM, Bhunjun CS, Hurdeal VG. Morphological approaches in studying fungi: collection, examination, isolation, sporulation and preservation. Mycosphere. 2020;11(1):2678-2754.

21. Elsayed EA, El Enshasy H, Wadaan MAM, Aziz R. Mushrooms: A potential natural source of anti-inflammatory compounds for medical applications. Mediators Inflamm. 2014; 2014: 805841.
22. Rehman G, Hamayun M, Iqbal A, Khan SA, Khan H, Shehzad A, Khan AL, Anwar S, Islam B, Lee IJ. Green synthesis and characterization of silver nanoparticles using Azadirachta indica seeds extract: In vitro and in vivo evaluation of antidiabetic activity. Molecules. 2021;26(12):3687.
23. Haleemkhan A, Naseem B, Vardhini B. Synthesis of nanoparticles from plant extracts. Int J Multidiscip Curr Acad Res. 2015;2:195-203.
24. Saranya S, Vijayarani K, Pavithra S. Green synthesis of iron nanoparticles using aqueous extract of Musa ornata flower sheath against pathogenic bacteria. Int J Pharm Sci Res. 2017;8(5):2241-2245.
25. Kalaiarasi R, Jayallakshmi N, Venkatachalam P. Phytosynthesis of nanoparticles and its applications. Plant Cell Biotechnol Mol Biol. 2010;11:1-16.
26. Ijaz M, Zafar MS, Al-Zereini WA, Al-Azawi AK, Al-Rawi M, Al-Hamadani H, Al-Ashekh M. Synthesis, characterization, and applications of iron oxide nanoparticles. Int J Health Sci. 2023;17(1):64-69.
27. Kumar V, Thakur M, Sharma P, Goutam SK, Singh S. Green synthesis of iron nanoparticles: Sources and multifarious biotechnological applications. Int J Biol Macromol. 2023; 253(Pt 5):127017.
28. Okka EZ, Ozturk S, Goksen G. Green synthesis and the formation kinetics of silver nanoparticles in aqueous Inula Viscosa extract. J Mol Liq. 2023;382: 121876.
29. Liang Y, Jiang L, Xu S, He S, Li J. Synthesis and characterization of Fe3O4 nanoparticles prepared by solvothermal method. J Mater Eng Perform. 2023;32:6465-6473.
30. Dhanasekaran D, Thajuddin N, Panneerselvam A. Extracellular biosynthesis, characterisation and in-vitro antibacterial potential of silver nanoparticles using Agaricus bisporus. J Exp Nanosci. 2013;8(4):579-588.
31. Rothen-Rutishauser B, Kuhn DA, Ali Z, Gasser M, Amin F, Parak WJ, Clift MJ. Nanoparticle-cell interactions: overview of uptake, intracellular fate and induction of cell responses. In: Gehr P, Mühlfeld C, Rothen-Rutishauser B, Blank F, editors. Nanoparticles in the Lung. Boca Raton: CRC Press; 2014. p. 153-170.
32. Xu W, Yang T, Li S, Du L, Chen Q, Li X, Dong J, Zhang Z, Lu S, Gong Y, Zhou L, Liu Y, Tan X. Insights into the synthesis, types and application of iron nanoparticles: The overlooked significance of environmental effects. Environ Int. 2022;158:106980.
33. Alahmad S, Alrebdi TA, Alshammari MT, Labban N. Nanofabrication and characterization of green-emitting N-doped carbon dots derived from pulp-free lemon juice extract. Opt Mater. 2023;139:113766.
34. Zhang Y, He X, Li Z, Zhang J, Luo Y, Li H. Bandgap engineering of two-dimensional perovskite semiconductors for high-performance solar cells. J Phys Chem C. 2018;122(17):9308-9317.
35. Chen Y, Fan Z, Luo Z, Liu X, Lai Z, Li B, Zong Y, Gu L, Zhang H. High-quality and water-resistant perovskite films for optoelectronic applications via a facile post-treatment process.

Nanoscale. 2019;11(13):6235-6242.
36. Wang Y, Zhang Y, Zhang P, Guo W. High-performance perovskite solar cells with enhanced stability via a facile interfacial passivation strategy. Sci Rep. 2020;10(1):12478.
37. Singh V, Haque S, Niwas R, Srivastava A, Pasupuleti M, Tripathi CKM. Strategies for fermentation medium optimization: An in-depth review. Biotechnol Adv. 2021;47:107731.
38. Patel SK, Kalia VC, Lee JK. Integrating strategies for sustainable conversion of waste biomass into dark-fermentative hydrogen and value-added products. ACS Omega. 2022;7(1):24-39.
39. Xu W, Yang T, Li S, Du L, Chen Q, Li X, Dong J, Zhang Z, Lu S, Gong Y, Zhou L, Liu Y, Tan X. Insights into the synthesis, types and application of iron nanoparticles: The overlooked significance of environmental effects. Environ Int. 2022;158:106980.
40. Poulsen PB, Buchholz K. History of enzymology with emphasis on food production. In: Whitaker JR, Voragen AGJ, Wong DWS, editors. Handbook of Food Enzymology. New York: Marcel Dekker; 2003. p. 11-20.
41. Sales PM, Souza PM, Simeoni LA, Silveira D. α-Amylase inhibitors: a review of raw material and isolated compounds from plant source. J Pharm Pharm Sci. 2012;15(1):141-183.
42. Tan Y, Li S, Li C, Liu S. Glucose adsorption and α-amylase activity inhibition mechanism of insoluble dietary fiber: Comparison of structural and microrheological properties of three different modified coconut residue fibers. Food Chem. 2023;418:135970.
43. Bamburowicz-Klimkowska M, Kasprzak A, Bystrzejewski M, Grudzinski IP. Characteristics of glucose oxidase immobilized on carbon-encapsulated iron nanoparticles decorated with polyethyleneimine. Polym Bull. 2023;80:1565-1586.
44. Saif S, Tahir A, Chen Y. Green synthesis of iron nanoparticles and their environmental applications and implications. Nanomaterials (Basel). 2016;6(11):209.
45. Ahmad H, Rajagopal K, Shah AH, Bhat AH, Venugopal K. Study of bio-fabrication of iron nanoparticles and their fungicidal property against phytopathogens of apple orchards. IET Nanobiotechnol. 2017;11(3):230-235.
46. Khezerlou A, Alizadeh-Sani M, Azizi-Lalabadi M, Ehsani A. Nanoparticles and their antimicrobial properties against pathogens including bacteria, fungi, parasites and viruses. Microb Pathog. 2018;123:505-526.